Zeitschrift fuer Angewandte Mathematik und Physik

Bifurcations of quasi-periodic dynamics: torus breakdown

--Manuscript Draft--

Manuscript Number:	ZAMP-D-13-00063R1
Full Title:	Bifurcations of quasi-periodic dynamics: torus breakdown
Article Type:	Original Research
Keywords:	quasi-periodic; tori; Neimark-Sacker; torus breakdown; strange attraction
Corresponding Author:	Ferdinand Verhulst, PhD University of Utrecht Utrecht, NETHERLANDS
Corresponding Author Secondary Information:	
Corresponding Author's Institution:	University of Utrecht
Corresponding Author's Secondary Institution:	
First Author:	Taoufik Bakri, PhD
First Author Secondary Information:	
Order of Authors:	Taoufik Bakri, PhD
	Ferdinand Verhulst, PhD
Order of Authors Secondary Information:	
Abstract:	To study the dynamics of quasi-periodic bifurcations, we consider a system of two nonlinearly coupled oscillators using averaging, continuation and numerical bifurcation techniques with numerical packages {\sc content}\cite{cont}, {\sc auto}\cite{auto} and {\sc matcont}\cite{matcont}. This relatively simple system displays considerable complexity. Assuming the internal resonance to be 1:2 we find a 2π-periodic solution which undergoes a supercritical Neimark-Sacker bifurcation, yielding a stable fixed symmetric torus. Choosing a route in parameter space, we show by numerical bifurcation techniques how the torus gets destroyed by dynamical and topological changes in the involved manifolds \cite{kraushink2}. The $1:6$-resonance turns out to be prominent and we detected a cascade of period doublings within the corresponding resonance tongue yielding a strange attractor. The phenomena agree with the Ruelle-Takens scenario \cite{RT} leading to strange attractors. Other periodic regimes are present in this system and there is interesting evidence that two different regimes interact with each other, yielding yet another type of large strange attractor. In this context certain π-periodic solutions emerge that are studied by continuation following the Poincar\'e-Lindstedt method using Mathieu-functions; when the implicit function theorem breaks down, the analysis is supplemented by numerical bifurcation techniques.
Response to Reviewers:	-The role of the semitrivial solution: We added on p. 9 that it is unstable and that increasing kappa, bifurcations arise. In the conclusion on p. 9 we added the condition for the existence of the 2 \pi- periodic solution. -Some confusion arose because there was a misprint on p. 20. The scaling of variable x is (epsilon)^{1/4 instead of -1/4.This gives the behaviour for small x. - The conjecture on I \pi-periodic solutions at the end of appendix 2 is summarized as

	conclusion on p.27. The evidence is very strong, both analytically and numerically,but not mathematically conclusive.

Bifurcations of quasi-periodic dynamics: torus breakdown

Taoufik Bakri*and Ferdinand Verhulst
Mathematisch Instituut, University of Utrecht
PO Box 80.010, 3508 TA Utrecht
The Netherlands

August 13, 2013

Abstract

To study the dynamics of quasi-periodic bifurcations, we consider a system of two nonlinearly coupled oscillators using averaging, continuation and numerical bifurcation techniques. This relatively simple system displays considerable complexity. Assuming the internal resonance to be $1:2$, we find a 2π-periodic solution which undergoes a supercritical Neimark-Sacker bifurcation, yielding a stable torus. Choosing a route in parameter space, we show by numerical bifurcation techniques how the torus gets destroyed by dynamical and topological changes in the involved manifolds [16]. The $1:6$-resonance turns out to be prominent in parameter space and we detected a cascade of period doublings within the corresponding resonance tongue yielding a strange attractor. The phenomena agree with the Ruelle-Takens scenario [22] leading to strange attractors. Other periodic regimes are present in this system and there is interesting evidence that two different regimes interact with each other, yielding yet another type of strange attractor. In this context certain π-periodic solutions emerge that are studied by continuation following the Poincaré-Lindstedt method using Mathieu-functions; when the implicit function theorem breaks down, the analysis is supplemented by numerical bifurcation techniques.

1 Introduction

The classical analysis of dissipative dynamics focuses on finding equilibria and periodic solutions and their stability. The theory of self-excited oscillations represents a well-known example. Considering systems with

*Now at TNO Built Environment and Geosciences, P.O. Box 49, 2600 AA Delft, The Netherlands

more than one degree of freedom, such as interacting nonlinear oscillators, this analysis must be supplemented by a study of quasi-periodic solutions and their bifurcations. Geometrically, quasi-periodic solutions correspond with tori, for instance two-frequency oscillations describe motion on a two-torus. What do we gain from geometric insight? It turns out that geometric pictures improve our understanding of the basic dynamics and in particular, bifurcational changes of the dynamics will correspond with changes in the geometry and vice versa. The purpose of this paper is to demonstrate this for a relatively simple model of two interacting oscillators. The surprise is that this model already contains a striking amount of complexity. The results agree with a visionary paper by Ruelle and Takens [22], see also [23], where the relation is suggested between turbulence in fluids and the bifurcation scenario in which equilibrium produces periodic solution, subsequently by bifurcation leading to a torus which in the next bifurcation produces a strange attractor.

Important insight in the dynamics of quasi-periodic bifurcations - tori bifurcation - were obtained for mappings in the early papers [1], [28] and [3]. Important new extensions of the theory can be found in [6], [32], [21] and [4]. The paper [4] is remarkable as it gives an extensive and early analysis of the wealth of phenomena encountered when three oscillators are interacting; these systems are more complex than the mechanical problem we will investigate.

Coninuation of tori is a delicate matter studied in [25]; [26] is related to our paper as it also exploits averaging and relative equilibria together with Fourier-Galerkin methods. The computation of Arnold tongues and the corresponding geometry is discussed in [27] and [8]. Extensive bibliographies can be found in [4], [7] and the other papers cited above.

In the case of system (1), the flow is four-dimensional and can be described by a three-dimensional map. The phenomena encountered in the dynamics of maps correspond with phenomena of differential equations but it is not so easy to validate identifications in actual examples. System (1) will provide an explicit example to illustrate the theory. As always, the set of Arnold tongues is very complex but it is dominated by one tongue corresponding with the $1 : 6$-resonance. Other interesting aspects are the presence of more than one attractor in the dynamical system and the use of Mathieu functions to perform continuation of a periodic solution.

The model

To illustrate torus bifurcations and show its relevance for engineering and physics we will consider the case of two interacting nonlinear oscillators, described by the eqations of motion:

$$\begin{cases} \ddot{x} + \delta x^2 \dot{x} + x + \gamma x^3 + axy = 0, \\ \ddot{y} + \kappa \dot{y} + 4y + bx^2 = 0. \end{cases} \tag{1}$$

This is a system of two coupled oscillators which, near the origin of phase-space, is in $1 : 2$ resonance; the nonlinear coupling is simple but contains the essential terms for this resonance case (essential in the sense of normal form theory). If $ab = 0$, there is no or one-sided coupling only; we will assume therefore $ab \neq 0$. By applying the linear transformation: $\tilde{x} = x$, $\tilde{y} = ay$, we can assume without loss of generality that the parameter $a = 1$. When computing averaging normal forms in the next section, we will put $a = 1$ which means that 4 parameters are involved.

The term $x + \gamma x^3$ represents the restoring force of the x-oscillator. As the bifurcation phenomena, discussed in what follows, take place for small values of γ, we do not expect much different behaviour for other restoring forces. The parameter γ however, is crucial as it causes the uncoupled, undamped x-oscillator ($\delta = a = 0$) to be asynchronous; we assume $\gamma > 0$. The parameter γ enables us to tune into the resonance (Arnold) tongues and to find interesting bifurcational behaviour; see again [6], [32] and [7] for references.

For the damping coefficients we assume $\delta, \ , \kappa > 0$. Adding linear damping to the first oscillator will not affect qualitatively the bifurcation scenario described below, it is omitted. Linear damping however would affect the stability of the origin and trigger an extra (unstable) periodic solution. For more details on the stability of the trivial equilibrium as well as the mechanical origin and applications of this system, we refer to [5]. An extension of the system with parametric exitation can be found in [19].

Note that system (1) possesses a $\mathbb{Z}_2$ (mirror) symmetry i.e. it is invariant with respect to the transformation:

$$T : \begin{pmatrix} x \\ y \end{pmatrix} \mapsto \begin{pmatrix} -x \\ y \end{pmatrix}.$$

Outline of the analysis

After briefly considering the less interesting case $b > 0$ in the next section, we will assume $b < 0$. Near the origin of phase-space, we expect the $1 : 2$ internal resonance to dominate the phase-flow, further away from the origin other resonances will appear. As discussed in [32] and [8], quasi-periodic solutions give rise to a dense occurrence of resonances and may even produce a "Cantorization" of the bifurcation sets. Note however that the immense complexity of this dynamics may simplify somewhat by the specific choice of relevant terms in the mechanical model and by the restriction to a location of phase-space of interest. We will demonstrate for our

model (1) that the dynamics of quasi-periodic bifurcations is indeed very complex, but can still be handled by analytic and numerical tools.

We proceed as follows. After performing scaling of the variables and the parameters, we start with averaging of the system to locate a relative equilibrium corresponding with a periodic orbit of which the stability can be determined. Varying the parameters of the system, in particular γ, the periodic solution undergoes a Neimark-Sacker bifurcation. We will study the dynamics after the Neimark-Sacker bifurcation has occurred, focusing on the dynamics within the $1:6$ resonance tongue. There exist an infinite number of other resonance tongues, but our numerical explorations in this part of phase space show that this tongue is the most prominent one.

The Neimark-Sacker bifurcation, which produces an attracting torus, is not captured by the averaging method as it occurs further away from the origin. The bifurcation diagram in Fig. 4 shows the presence of a $1:6$ resonant tongue in the parameter region of our interest. The Poincaré section of the flow, which is three-dimensional, is examined by projection on a plane. A numerical study using the software packages AUTO [12] and CONTENT [18], see also [9], [10] and [11], shows how within the $1:6$ resonance tongue, through a route in parameter space, the emerging torus becomes nonsmooth before it breaks down, leading to a strange attractor. This loss of smoothness occurs before the phase-locked periodic solution has lost normal hyperbolicity and has undergone a period doubling. Hereafter, a cascade of period doublings in the $1:6$ resonant tongue in the direction orthogonal to the unstable manifolds of the saddles follows, after which a nontrivial limit set emerges and a strange attractor is born. This is one of the known routes to chaos. Other scenarios of torus breakdown are also possible, such as for example the loss of normal hyperbolicity or the occurrence of heteroclinic tangencies followed by homoclinic tangencies leading to Smale horseshoe dynamics and chaos. In our case, we show explicitly how the torus is destroyed by following the changes in the involved manifolds.

But this is not the only phenomenon of interest. Other periodic regimes, symmetrically coupled π-periodic solutions, are present in the system, somewhat further from the origin; they are analysed, their emergence is explained and a bifurcation diagram is given. This analysis starts with another rescaling and using the Poincaré-Linstedt method based on Mathieu functions. In itself an unusual application, it helps to analyse the bifurcation phenomena of system (1). Of course, this study can be extended to other (minor) resonance tongues and transitions in the spirit of [32] and [8].

There are two cases which should be distinguished, namely the case $ab > 0$ and the case $ab < 0$. The dampings are positive, $\delta, \kappa > 0$. We shall often use system (1) in the form of a first-order system; with $a = 1$ it

becomes:

$$\begin{cases} \dot{x}_1 = x_2, \\ \dot{x}_2 = -x_1 - \delta x_1^2 x_2 - \gamma x_1^3 - x_1 y_1, \\ \dot{y}_1 = y_2, \\ \dot{y}_2 = -4y_1 - \kappa y_2 - b x_1^2. \end{cases} \tag{2}$$

2 The flow near equilibria if $b > 0$

If $b > 4\gamma$, there are three critical points:

$$(0,0,0,0), \text{ and } (\pm 2/\sqrt{b-4\gamma}, 0, -b/(b-4\gamma), 0),$$

so nontrivial equilibria exist if $b > 4\gamma$.

2.1 The equilibrium at $(0,0,0,0)$

The origin has the following eigenvalues:

$$\lambda_{1,2} = \pm i, \ \lambda_{3,4} = \frac{-\kappa \pm \sqrt{\kappa^2 - 16}}{2}.$$

The stability is not determined by linear analysis so we reduce the flow to the two-dimensional centre manifold and normalise it in the usual way, see [17], chapter 5. We omit the technical details.

Using polar variables ρ, ϕ in the two-dimensional centre manifold, we find for the normal form:

$$\dot{\rho} = \operatorname{sgn}(l_1(0))\rho^3 + O(\rho^4), \ \dot{\phi} = 1 \tag{3}$$

with $l_1(0)$ the first Lyapunov coefficient:

$$l_1(0) = -\frac{\delta}{2} - \frac{b}{4\kappa}. \tag{4}$$

Clearly we have $l_1(0) < 0$ in the case $b > 0$, the origin is stable.

2.2 Global attraction if $0 < b < 4\gamma$

In this case, the origin is the only equilibrium. It is nontrivial that system (2) can be transformed to a Hamiltonian system if $\kappa = \delta = 0$. We use the following transformation of coordinates

$$(\tilde{x}_1, \tilde{x}_2, \tilde{y}_1, \tilde{y}_2) = (x_1, b x_2, y_1, \frac{y_2}{2}). \tag{5}$$

Omitting the tildes, the Hamiltonian has the following form

$$H(x_1, x_2, y_1, y_2) = \frac{b}{2}\left(x_1^2 + \left(\frac{x_2}{b}\right)^2\right) + \left(y_1^2 + y_2^2\right) + \frac{\gamma b}{4}x_1^4 + \frac{b}{2}x_1^2 y_1.$$

To show that the origin is a global attractor, we can directly use the Hamiltonian or a Lyapunov function of the form:

$$V(x_1, x_2, y_1, y_2) = 2x_1^2 + 2x_2^2 + \frac{4}{b}y_1^2 + \frac{1}{b}y_2^2 + 2x_1^2 y_1 + \gamma x_1^4. \tag{6}$$

Computing the orbital derivative of this Lyapunov function yields:

$$\frac{dV}{dt} = -4\delta x_1^2 x_2^2 - \frac{2\kappa}{b}y_2^2$$

Clearly the orbital derivative is negative if $x_1,\ x_2$ and y_2 do not vanish. The Lyapunov function can also be written as

$$V(x_1, x_2, y_1, y_2) = 2x_1^2 + 2x_2^2 + \frac{1}{b}y_2^2 + \left(\frac{\sqrt{b}}{2}x_1^2 + 2\sqrt{\frac{1}{b}}y_1\right)^2 + \left(\gamma - \frac{b}{4}\right)x_1^4, \tag{7}$$

which is positive definite. It is easy to see that the phaseflow is transversal to the manifold $x_1 = y_2 = 0$ and the manifold $x_2 = y_2 = 0$. We conclude:

Proposition 1 *If $0 < b < 4\gamma$ the equilibrium at the origin is a global attractor.*

2.3 The nontrivial equilibria if $b > 4\gamma > 0$

We shall argue that the symmetrical equilibria have a saddle character and that no bifurcation will involve these equilibria, in particular no Hopf bifurcation.

Proposition 2 *If $b > 4\gamma$ the two nontrivial symmetrical fixed points exist and have at least one negative eigenvalue (λ_-) and exactly one positive (λ_+). Furthermore the eigenvalues never become zero or cross the imaginary axis and we have the following asymptotic estimate:*

$$\lambda_+ = O(\Delta), \qquad (\Delta \to 0).$$

Where $\Delta = b - 4\gamma$.

Sketch of a proof
Consider the equilibrium $(2/\sqrt{b-4\gamma}, 0, -b/(b-4\gamma), 0)$, the reasoning for the other equilibrium is analogous following the $\mathbb{Z}_2$ symmetry. Linearising system (2) near this equilibrium yields a matrix with characteristic polynomial:

$$P(\lambda) = \lambda\left(\frac{4\delta}{\Delta} + \lambda\right)\left[\lambda(\lambda + \kappa) + 4\right] + \frac{8\gamma\lambda}{\Delta}(\lambda + \kappa) - 8.$$

We easily see that $P(0) = -8$, $\lim_{\lambda \to \pm\infty} P(\lambda) = +\infty$. There are at least two real roots of this quartic polynomial. Elementary analysis of the polynomial gives the desired result. In particular, to show that the eigenvalues never become purely imaginary we compute $P(i\omega)$ with $\omega \in \mathbb{R}^+$. Putting $P(i\omega) = 0$ produces equations without real solutions for ω. Another result of this analysis is:

Proposition 3 *The two nontrivial symmetrical equilibria have a one-dimensional unstable manifold and a three-dimensional stable manifold.*

3 The flow near the equilibria if $b < 0$

The scale transformation (5) clarifies the part played by the sign of parameter b. It produces in the x-oscillator a damping term of the form $\delta b x_1^2 x_2$ which for $\delta b < 0$ may produce self-excited oscillations.

In this section, we will localize near equilibria to find a periodic solution that can be continued in parameter space. We put again $a = 1$; if $b < -2\kappa\delta < 0$, the origin is in this case unstable as the first Lyapunov coefficient $l_1(0)$ is positive, see equation (4), so the local dynamics will be more interesting. We shall use averaging-normalisation which enables us to locate periodic solutions for which existence and precise error estimates are known.

3.1 Scaling and first order averaging

Consider system (1) in the vicinity of the origin; with ε a small, positive parameter, we introduce the following scaling (for more details about this choice see [5]):

$$x = \sqrt{\varepsilon}\bar{x},\ y = \varepsilon\bar{y},\ b = \varepsilon\bar{b},\ \kappa = \varepsilon\bar{\kappa}. \tag{8}$$

Another scaling will produce a different localisation and other phenomena, see section 5. The parameters δ and γ are assumed not to be dependent on ε. Introducing scaling (8) into system (1) and omitting the bars yields:

$$\begin{cases} \ddot{x} + x + \varepsilon x y + \varepsilon(\delta x^2 \dot{x} + \gamma x^3) = 0, \\ \ddot{y} + 4y + \varepsilon\kappa\dot{y} + \varepsilon b x^2 = 0. \end{cases} \tag{9}$$

The next steps are the usual ones in averaging approximations; see for instance [30], chapter 11. We introduce the following amplitude-phase transformation:

$$\begin{cases} x(t) = R_1(t)\cos(t + \phi(t)) & \dot{x}(t) = -R_1(t)\sin(t + \phi(t)) \\ y(t) = R_2(t)\cos(2t + \psi(t)) & \dot{y}(t) = -2R_2(t)\sin(2t + \psi(t)) \end{cases}$$

Averaging the resulting slowly varying system yields:

$$\begin{cases} \dot{R}_1 &= \varepsilon R_1\{\frac{1}{4}R_2\sin(2\phi-\psi)-\frac{\delta}{8}R_1^2\} \\ \dot{\phi} &= \varepsilon\{\frac{1}{4}R_2\cos(2\phi-\psi)+\frac{3}{8}\gamma R_1^2\} \\ \dot{R}_2 &= \frac{\varepsilon}{2}R_2\{-bR_1^2/(4R_2)\sin(2\phi-\psi)-\kappa\} \\ \dot{\psi} &= \frac{\varepsilon}{2}\{bR_1^2/(4R_2)\cos(2\phi-\psi)\} \end{cases} \tag{10}$$

As usual, the dimension of this system can be reduced by introducing the phase variable $\theta = 2\phi - \psi$. The system becomes

$$\begin{cases} \dot{R}_1 &= \varepsilon R_1\{\frac{1}{4}R_2\sin\theta-\frac{\delta}{8}R_1^2\} \\ \dot{R}_2 &= \frac{\varepsilon}{2}R_2\{-bR_1^2/(4R_2)\sin\theta-\kappa\} \\ \dot{\theta} &= \varepsilon\{\frac{1}{2}R_2\cos\theta+\frac{3}{4}\gamma R_1^2-bR_1^2/(8R_2)\cos\theta\} \end{cases} \tag{11}$$

Nontrivial critical points (equilibria) of system (11) will correspond with 2π-periodic, phase-locked solutions of the original system (9), see [24]; we call them relative equilibria. First, we remark that putting the righthand-sides of the first two equations to zero and looking for nontrivial solutions produces the following system:

$$A\begin{pmatrix} R_1^2 \\ R_2 \end{pmatrix} = \begin{pmatrix} 0 \\ 0 \end{pmatrix}$$

with the matrix

$$A = \begin{pmatrix} -\delta/8 & 1/4\sin\theta \\ -b/4\sin\theta & -\kappa \end{pmatrix}.$$

If the matrix A is invertible then it is clear that the trivial solution is the only solution. We therefore require that $\det(A) = 0$. A necessary condition for the existence of nontrivial solutions to the reduced system (11) reduces then to

$$\sin\theta = \pm\sqrt{\frac{-2\kappa\delta}{b}}.$$

Note that system (11) can have nontrivial equilibrium solutions only if $b < -2\kappa\delta < 0$. Solving the equations for equilibrium yields:

$$\begin{cases} R_2 &= -\dfrac{b}{4\kappa}R_1^2\sin\theta \\ R_1 &= \sqrt{\dfrac{-8\kappa^2\cot\theta}{12\kappa\gamma-b\sin 2\theta}} \end{cases} \tag{12}$$

provided that the damping coefficients κ, δ are positive. It follows from the first equation of system (12) that $\sin\theta \geq 0$. If $\kappa = 0$, and $\delta \neq 0$ then system (11) has a continuous family of nontrivial critical points and therefore we

cannot deduce the existence of periodic solutions. However one can easily see from the original equations of motion (1) that a family of semitrivial solutions exists. The $x-$oscillator is at rest while the $y-$oscillator is a simple harmonic oscillator. On the other hand, if $\delta = 0$, and $\kappa \neq 0$ then there is a family of semitrivial solutions where the $y-$oscillator is at rest while the $x-$oscillator oscillates. The period is in this case dependent on the initial condition. We will see in section 5.1 that this semi-trivial solution is unstable if $\kappa = 0$, bifurcations arise as κ grows.

Conclusion

The original system (9) has an isolated $2\pi-$periodic solution provided γ is large enough, $\kappa, \delta > 0$, $b < -2\kappa\delta$ and $\theta \in (\pi/2, \pi)$. We have from system (12) the requirement

$$12\kappa\gamma > b \sin 2\theta.$$

3.2 Stability of the $2\pi-$periodic solution

Linearising the reduced averaged system (11) around the nontrivial critical point and analysing the corresponding Routh-Hurwitz system of equations, see [14], yields that the nontrivial relative equilibrium is asymptotically stable no matter what the parameters are; see appendix 1 for the stability analysis. This is quite surprising. It implies that the corresponding periodic solution of system (9) is also asymptotically stable provided its amplitude is $O(1)$ with respect to ε. However, using γ as a control parameter, one can numerically find that the amplitudes of the periodic solution R_1 and R_2 can become fairly large, cf. system (12), and consequently grow beyond the domain of validity of the averaging method. In that case the stability of the periodic solution can be destroyed by bifurcations which are not detected by the normal form. We shall therefore return in what follows to the original system (2) and study numerically the flow and the bifurcations involved. This study reveals very rich dynamics including torus break-down, and chaotic behaviour .

4 Numerical continuation of the (symmetric) periodic solution

In this section we will perform numerical continuation and compute Poincaré sections based on the original system (1).

4.1 The Neimark-Sacker bifurcation

The following representative parameters, with respect to the original system (2), have been used in our numerical analysis: $a = 0.5$, $b = -0.5$, $\delta =$

0.4, $\kappa = 0.1$. We use the software package CONTENT [18] to continue the periodic solution, detected by the normal form system (11) as a relative equilibrium, with respect to the parameter γ. Numerical experiments show that interesting phenomena occur for certain positive values of the parameter γ; we therefore start at $\gamma = 0.2$ and decrease continuously this parameter.

A supercritical Neimark-Sacker bifurcation has been detected at the critical value $\gamma_{NS} \approx 0.096$. In the computations via periodic normalisation of MATCONT [20] or [17], this is determined by a so-called 'normal form coefficient'; in this case the coefficient is small but negative $C_{NS} = -7.225 \times 10^{-7}$, see Fig. 1 below. Below but near this critical value of γ a stable smooth torus is present. See the numerically computed projected Poincaré section in Fig. 2. Continuing the unstable cycle after the Neimark-Sacker bifurcation with respect to the parameter γ does not yield any other bifurcations until, at the parameter value $\gamma = 0.0892$, the torus is destroyed and a strange attractor emerges; see Fig. 3. In order to better understand the mechanism behind the birth of this strange attractor, we will go into more details of the analysis of the bifurcation diagram in the involved parameter region.

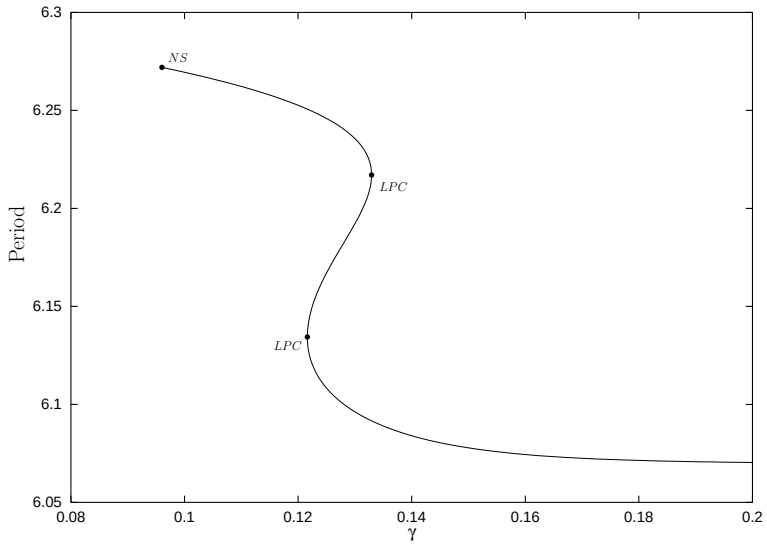

Figure 1: Figure generated by CONTENT. Plot of the period which is not far from 2π against the parameter γ. The periodic solution is continued with respect to the parameter γ starting at the value 0.2. LPC stands for Limit Point Cycle (fold) bifurcation and NS stands for the Neimark-Sacker bifurcation happening near $\gamma = 0.096$.

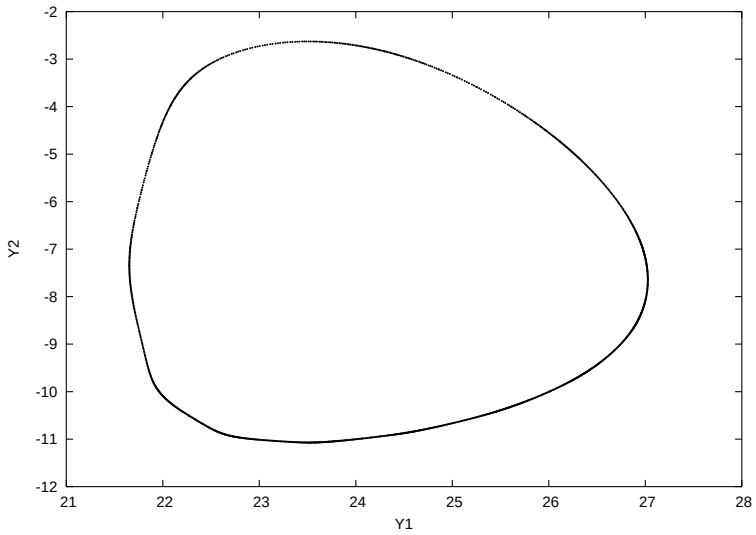

Figure 2: Poincaré section, using $\Sigma = \{(0, x_2, y_1, y_2)^T, x_2, y_1, y_2 \in \mathbb{R}\}$ as cross section, projected onto the $y_1 y_2$ plane with $\gamma = 0.092$. The smooth closed curve corresponds with the stable and smooth $\mathbb{T}_2$ torus.

4.2 Resonance tongues and cascade of period doublings

In the parameter region where the smooth torus exists, between $\gamma = 0.096$ and 0.089, there are regions where phase locking occurs, the so called Arnold tongues. This has strong dynamical consequences. Here the torus, in the case it still exists, becomes resonant, yielding simultaneously stable and unstable periodic motion. This happens for example at the parameter value $\gamma = 0.09185$ yielding a stable and an unstable $1:6$ periodic solution on the torus. The two periodic solutions collide and disappear through a fold (saddle-node) bifurcation along the boundaries of the tongue. Using the software package AUTO [12] for the shape of the tongues and CONTENT [10] for the multipliers, and taking the coupling parameter b as a second control parameter, we were able to compute the bifurcation diagram Fig. 4 presented below. First the Neimark-Sacker curve is computed by continuation, then the locus of the folds involving the $1:6$ periodic orbits is computed yielding the boundaries F of the $1:6$ resonance tongue. Fig. 4 shows a part of the bifurcation diagram. The left and right boundaries of the $1:6$ resonance tongue correspond to fold curves F. There, the saddle (unstable periodic motion) and the node (stable periodic motion) collide and disappear. The lower boundary of the tongue corresponds to the first period doubling bifurcation of the node. The stable cycle of period 6 then becomes unstable and a stable period 12 cycle emerges. Because of the $\mathbb{Z}_2$ symmetry there are two of these cycles. Note that for Chenciner bifurcation , indicated by Ch, one also uses 'degenerate Hopf bifurcation'; it is a

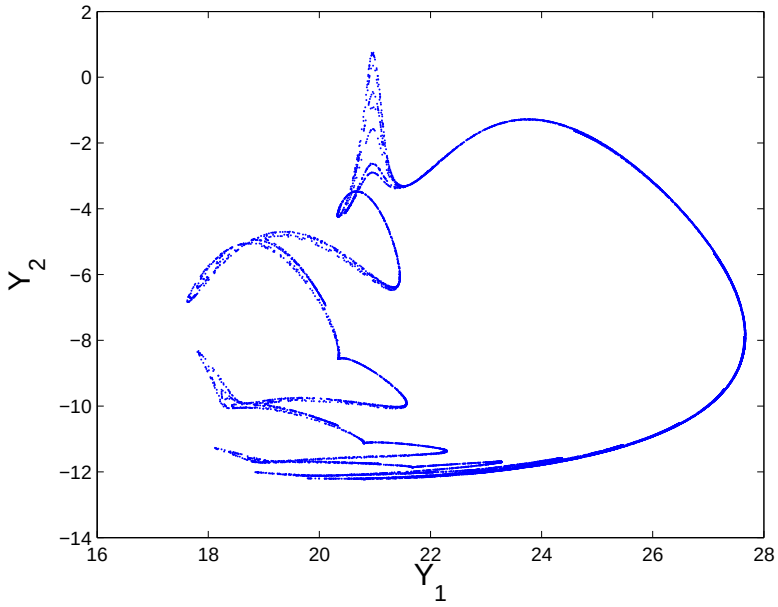

Figure 3: Poincaré section, using $\Sigma = \{(0, x_2, y_1, y_2)^T, x_2, y_1, y_2 \in \mathbb{R}\}$ as cross section, projected onto the $y_1 y_2$ plane with $\gamma = 0.0892$. The closed curve, corresponding with a torus, no longer exists. A strange attractor emerges instead. Its Kaplan-Yorke dimension $d_{KY} \approx 2.32$.

codimension two bifurcation with two purely imaginary eigenvalues and one zero.

Keeping the parameter $b = -0.5$ constant and letting the parameter γ decrease, we "hit" the $1:6$ resonance tongue three times: at $\gamma = 0.091902$, $\gamma = 0.09173$, and $\gamma = 0.09035$. At the parameter value $\gamma = 0.09184$, further away from the period doubling curve, the projected Poincaré section shows a smooth closed curve, see Fig. 5. As γ decreases, we leave the tongue and enter a parameter region where complex dynamics occurs alternated with periodic motion. Leaving the tongue but remaining in the neighborhood, the torus is no longer resonant but still smooth. The projected Poincaré section shows a closed curve with no saddles or nodes on it. Before reentering the $1:6$ resonance tongue again, the torus gets destroyed more often and according to different scenarios; strange attractors sometimes emerge from these destructions. Although the dynamics in this region is rich it does not yet explain the origin of the strange attractor in Fig. 3. We shall therefore focus in what follows on the $1:6$ resonance tongue as the strange attractor emerges within it. Entering the tongue for the second time, but now closer to the period doubling curve, at $\gamma = 0.09$ the Poincaré section shows a closed curve which seems to have lost its smoothness; see Fig. 6. How-

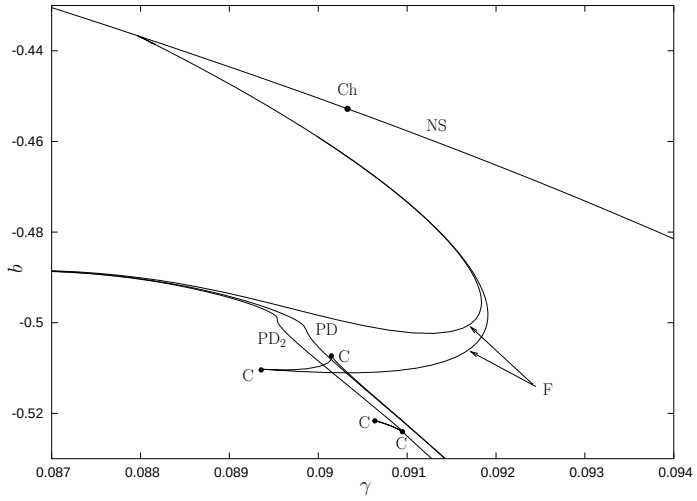

Figure 4: Bifurcation diagram in the case $ab < 0$ in the vicinity of the $1:6$ resonance tongue based on AUTO, the bifurcations are analysed by MATCONT. The tongue is quite narrow and is bounded from below by the period-doubling (PD) curve. The left and right boundaries of the tongue correspond to fold curves (F). Here the period 6 saddle and node solutions collide and disappear. (NS) stands for Neimark-Sacker bifurcation, (Ch) stands for Chenciner bifurcation (also called 'degenerate Hopf bifurcation) and (C) corresponds to a cusp bifurcation.

ever, considering the Lyapunov exponents, the dynamics is not strange. Decreasing the parameter γ further we hit the period doubling curve at approximately the parameter value $\gamma = 0.0897934$. At $\gamma = 0.0897$ i.e. after the first period doubling, the numerically computed Poincaré section shows a closed curve but with complicated geometry. See Fig. 7. When γ drops below this critical value, a cascade of period doublings follows respectively at $\gamma = 0.08954709$, $\gamma = 0.08954241$, $\gamma = 0.08954129$ etc. yielding ultimately the strange attractor mentioned above, see Fig. 3.

Remark

Note that if $a = \gamma = 0$, we have a synchronous oscillator which is a very degenerate case. Introducing positive values of the parameters γ and a, we couple to an asynchronous oscillator and trigger resonance phenomena which yield the invariant sets we encountered. One may look at the parameter γ as a source of chaos phenomena. Indeed, when the parameter γ equals zero, the system is either chaotic or its orbits are unbounded.

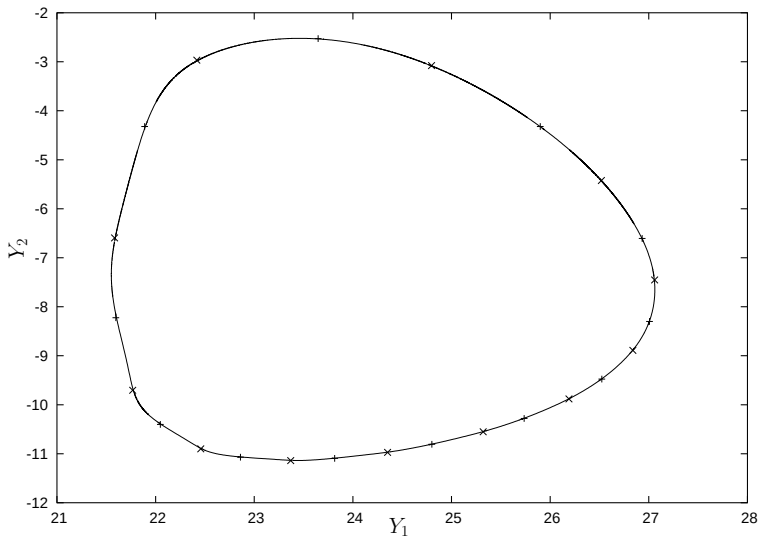

Figure 5: Numerically computed projection of Poincaré section in the $1:6$ resonance tongue: $\gamma = 0.09184$ showing a smooth closed curve corresponding to a torus. The closed curve is obtained by numerically computing the unstable manifolds of the saddles. Because of the $1:2$-resonance, the Poincaré-map in the y_1, y_2-plane produces for the stable (indicated by $+$) and the unstable (indicated by $\times$) periodic solutions 12 fixed points each.

4.3 Birth of the strange attractor

We will examine how the birth of a strange attractor happens as a consequence of a cascade of period doublings. Before the period doubling takes place, closer to the boundary of the $1:6$ resonance tongue at $\gamma = 0.0903$, the unstable manifold of the saddle wraps around the node, showing that a heteroclinic crossing has already occurred. This means that the unstable manifold of the saddle has crossed the nonleading stable manifold of the node, see Fig. 8.

The phenomenon of heteroclinic crossings within the tongues has been studied in detail in the literature for maps, but not often for differential equations where the mechanisms are more hidden. At this stage the closure of the invariant set consisting of the union of the unstable manifolds of the saddles is no longer homeomorphic to the circle. In other words, the torus has already been destroyed. Denoting the multipliers of the nodes by μ_i with $\mu_0 = 1 \geq |\mu_1| \geq |\mu_2| \geq |\mu_3|$, we found at $\gamma = 0.0903$ that $\mu_1 > |\mu_2|$, $\mu_2 < 0$ and $\mu_3 = O(10^{-17}) < 0$. This means that the Poincaré map is contracting following the direction of two eigenvectors. Hence this map can be well approximated by a two dimensional map. An extensive study of this kind of planar maps can be found in [6], [32] and [8]. In order to

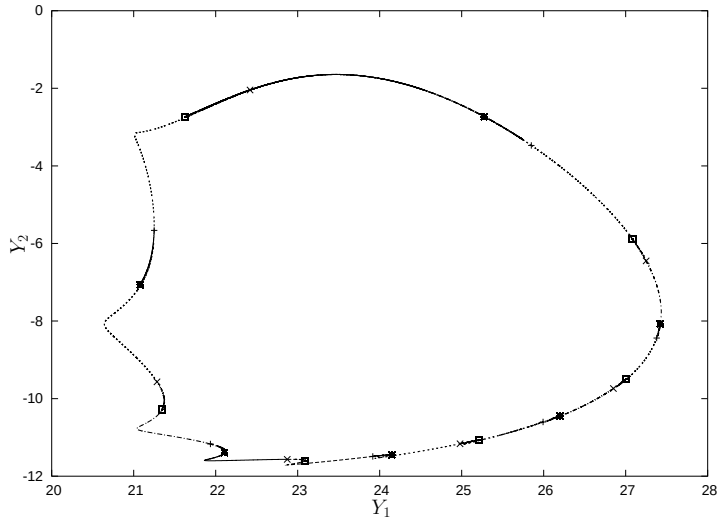

Figure 6: Numerically computed projection of Poincaré section in the $1:6$ resonance tongue, closer to the period-doubling curve: $\gamma = 0.09$ showing loss of smoothness. For a remark on the fixed points see the caption of Fig. 5.

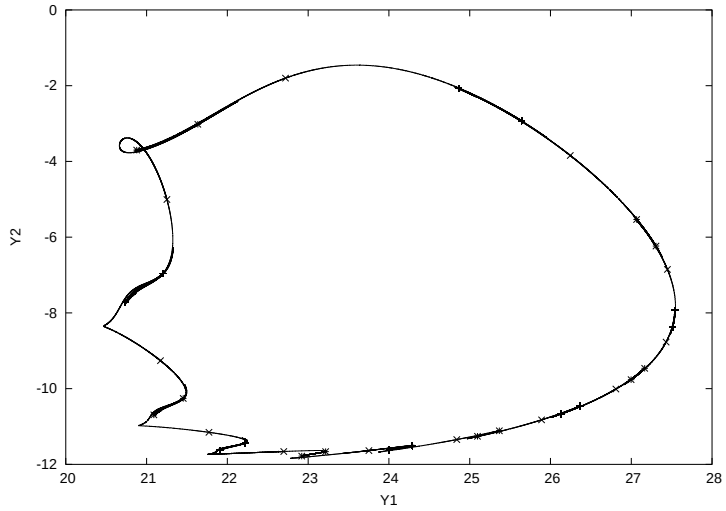

Figure 7: Numerically computed projection of Poincaré section in the $1:6$ resonance tongue, after the period-doubling has occurred: $\gamma = 0.0897$. For a remark on the fixed points see the caption of Fig. 5.

better understand how the unstable manifold in Fig. 8 wraps around the node, a sketch is given Fig. 9 below.
As the parameter γ decreases further, loss of normal hyperbolicity (NH) occurs at approximately the value $\gamma = 0.09022$. Here we have $\mu_1 = |\mu_2|$. At

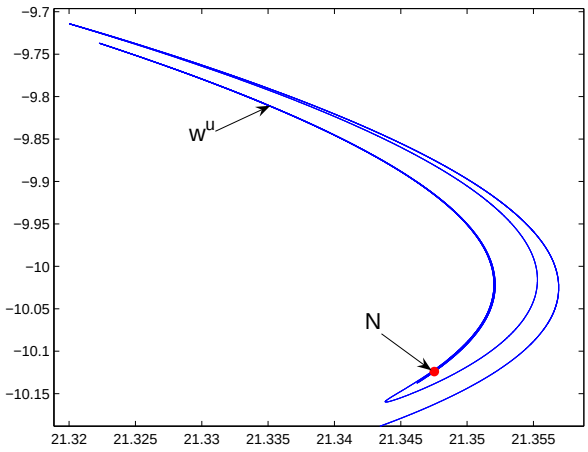

Figure 8: Numerically computed unstable manifold of the saddle wrapping around the node in the $1:6$ resonance tongue $\gamma = 0.0903$, $b = -0.5$.

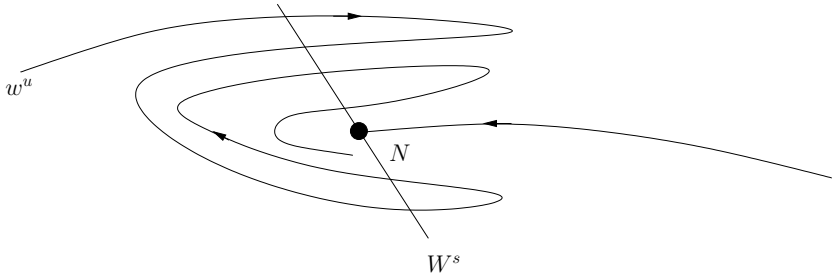

Figure 9: Sketch of how the unstable manifold of the saddle (w^u) wraps around the node (N) as it crosses the nonleading stable manifold (W^s) of the node corresponding to the negative multiplier μ_2. Because of the negative sign of μ_2 the unstable manifold w^u , when it crosses W^s, it must cross it in this manner.

the parameter value $\gamma = 0.0897934$ the nonleading multiplier of the node becomes equal to -1 yielding a period doubling of the period 6 stable cycle in the direction of W^s. See Fig. 10 below. In other words, The cascade of period doublings that occurs here happens in the direction of W^s. After this cascade of period doublings a strange attractor emerges.
This is followed by an interesting phenomenon: an inverse cascade of strange attractors. At each step n of the cascade we have a strange attractor consisting of $2^n \times 6$ parts. Following the inverse cascade in parameter-space, at each step the $2^n \times 6$ parts strange attractor merges to form a $2^{n-1} \times 6$ parts strange attractor until we end up with a strange attractor consisting

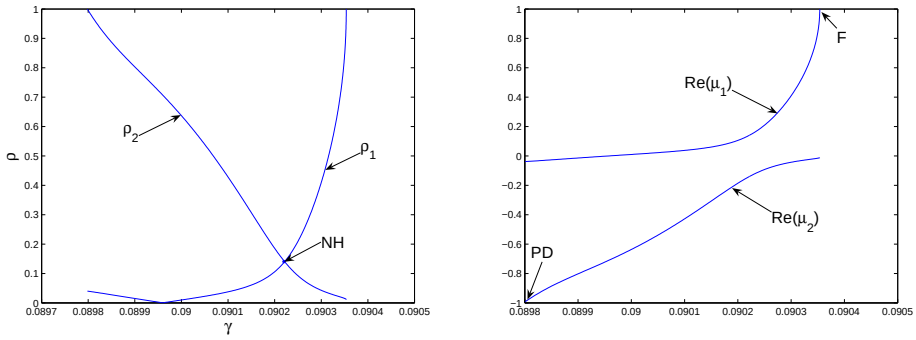

Figure 10: Plot of the modulus of the multipliers (left) and of the real part (right) against the parameter γ. We see that as γ tends to 0.09035, μ_1 tends to 1 (fold bifurcation) corresponding to the boundary of the tongue. When γ tends to 0.08979, μ_2 tends to -1 yielding a period doubling of the node in the direction of W^s. NH (where the multipliers are equal) stands for loss of normal hyperbolicity.

of six parts. Ultimately a 'large' strange attractor consisting of one part only emerges, see Fig. 11 below. This 'large' attractor ultimately evolves towards the one observed in Fig. 3. See again the references in the context of maps.

5 Dynamics away from the origin

We shall now proceed, again for $b < 0$, with a brief study of the dynamics of the system much further from the origin, showing co-existing but different dynamics; also, these regimes show complicated interaction with the ones already studied.
System (1) has for instance periodic regimes coexisting with the one studied previously. There is a pair of symmetrically coupled $\pi-$periodic solutions, see Fig. 12.

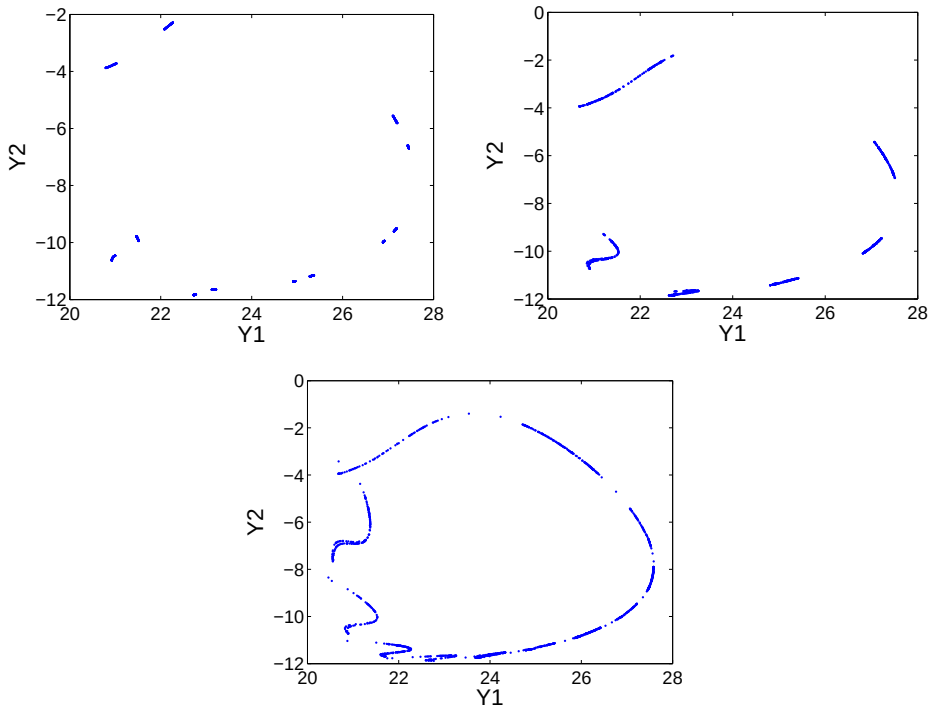

Figure 11: Inverse cascade of strange attractors ending with a one piece large strange attractor corresponding to the parameter values $\gamma = 0.08954$ (upper left), $\gamma = 0.08952$ (upper right) and $\gamma = 0.08951$ (projection on (y_1, y_2)-plane).

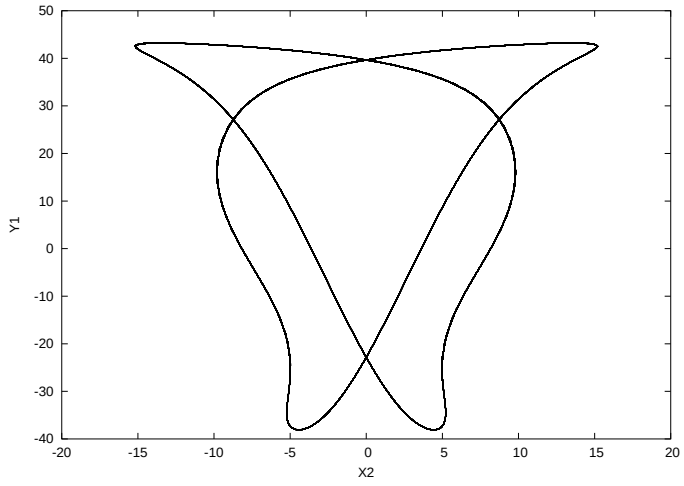

Figure 12: Two stable, symmetrically coupled π-periodic orbits, $\gamma = 0.25$ (projection on (x_2, y_1)-plane).

5.1 The emergence of the two stable symmetrically coupled π-periodic solutions

In order to understand the emergence of the π-periodic solutions, we continue them with respect to the damping parameter κ. A forward continuation yields a fold bifurcation at $\kappa = 0.11086$, then as the parameter κ tends to zero, the unstable orbit tends to a degenerate situation in the sense that the amplitude of the x-oscillator tends to zero whereas that of the y-oscillator tends to a specific value c. We found

$$c = \lim_{\kappa \to 0} [y] = 12.866. \tag{13}$$

Here the brackets are used to refer to the amplitude. It turns out that this value is such that the Mathieu-sine function MathieuS$(1, -[y]/2, t)$ is π-periodic. Note that in this case the Mathieu equation is hidden in the x-oscillator, see system (1) with $a = 1$. This is quite remarkable as the amplitude of the y-oscillator seems arbitrary. The question now is why does the amplitude of the y-oscillator in the normal mode plane $x = \dot{x} = 0$ tends to this specific value as the damping parameter κ tends to zero? Somehow, the $x-$oscillator is still involved. This suggests an explanation by the presence of a hidden scaling in the $x-$oscillator. To check this hypothesis, we introduce the following scaling into system (1), with $a = 1$, $x = \sqrt{\varepsilon}\hat{x}$, $\kappa = \varepsilon\hat{\kappa}$. Omitting the hats for notational simplicity we find:

$$\begin{cases} \ddot{x} + (1+y)x + \varepsilon\delta x^2\dot{x} + \varepsilon\gamma x^3 = 0, \\ \ddot{y} + \varepsilon\kappa\dot{y} + 4y + \varepsilon b x^2 = 0. \end{cases} \tag{14}$$

Taking the parameters $\varepsilon = 0.1$, $\kappa = 1$ and keeping the other parameters unchanged, we perform a continuation of the π-periodic solution with respect to the parameter ε. First, as expected, a fold bifurcation is detected, then as ε tends to zero, the amplitude of the $x-$oscillator seems to tend to infinity, whereas that of the $y-$oscillator tend to the limit c of equation (13). We note that a plot of the amplitude $[x]$ against $\varepsilon^{(-1/4)}$ yields a straight line with slope equal to 7.07, see Fig. 13. This means a scaling of magnitude $O(\varepsilon^{1/4})$ is more appropriate to use in this case.

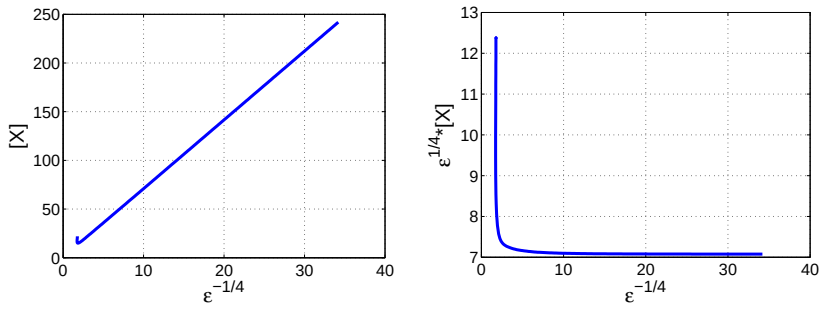

Figure 13: Plot of the numerically obtained amplitude of the (scaled) $x-$oscillator against $\varepsilon^{(-1/4)}$ yielding a straight line with slope approximately equal to 7.07. This suggests an $O(\varepsilon^{1/4})$ scaling in the original system (1) with $a = 1$.

5.2 The Poincaré-Lindstedt method

We shall use the Poincaré-Lindstedt method (PL-method), which is in essence continuation based on the implicit function theorem, to add to our understanding of the origin of the $\pi-$periodic solutions. For more details about the method, we refer to [15] or [30], Chapter 10. Some technical aspects of the Mathieu-functions that we will use are summarised in appendix 2. In [13] tori are studied for Mathieu type perturbations in dynamics, but in our case it is the Mathieu dynamics that is to be perturbed. Note also that averaging-normalisation is confronted by the problem that one solution branch of the Mathieu dynamics contains periodic functions while the other branch contains unbounded solutions. For the Poincaré-Lindstedt method we restrict the expansion to the periodic branch.
Introduce the following scaling into system (1) with $a = 1$,

$$x = \varepsilon^{\frac{1}{4}}\hat{x}, \qquad \kappa = \varepsilon\hat{\kappa}.$$

Omitting the hats for notational simplicity we have:

$$\begin{cases} \ddot{x} + (1+y)x + \sqrt{\varepsilon}\delta x^2\dot{x} + \sqrt{\varepsilon}\gamma x^3 = 0, \\ \ddot{y} + 4y + \sqrt{\varepsilon}bx^2 + \varepsilon\kappa\dot{y} = 0. \end{cases} \tag{15}$$

If $\varepsilon = 0$, the $y-$oscillator is just the harmonic oscillator. As system (15) is autonomous, we can assume without loss of generality that $\dot{y}(0) = 0$. This assumption leads to the conclusion that the unperturbed ($\varepsilon = 0$) $x-$oscillator is then governed by the Mathieu equation. Expand $x(t)$ and $y(t)$ as follows:

$$\begin{cases} x(t) = x_0(t) + \sqrt{\varepsilon}x_1(t) + \varepsilon x_2(t) + O(\varepsilon^{3/2}), \\ y(t) = y_0(t) + \sqrt{\varepsilon}y_1(t) + \varepsilon y_2(t) + O(\varepsilon^{3/2}), \end{cases} \tag{16}$$

and, after corresponding expansion, solve the system (15) for $x_0(t)$ and $y_0(t)$. Inspired by the numerical analysis above we put

$$y_0(t) = c\cos 2t, \tag{17}$$

where c is as in equation (13). Putting this into the equation of the $x-$oscillator and requiring x_0 to be $\pi-$periodic yields

$$x_0(t) = x_{00}\text{MathieuS}(1, -c/2, t), \tag{18}$$

with x_{00} still unknown and MathieuS$(1, -c/2, t)$ defined as the solution of the following initial value problem:

$$\begin{cases} \ddot{x} + (1 + c\cos 2t)x = 0, \\ x(0) = 0, \quad \dot{x}(0) = 1. \end{cases}$$

Note that $x_0(t)$ is odd. This property will be used later when imposing the periodicity condition.
The unperturbed solution is in this case $\pi-$periodic. For $\varepsilon \neq 0$ we expect the period to change slightly. Introduce therefore the following time variable

$$\theta = \omega t, \quad \text{with} \quad \omega^{-2} = 1 - \sqrt{\varepsilon}\eta, \tag{19}$$

where

$$\eta = \eta_0 + \sqrt{\varepsilon}\eta_1 + O(\varepsilon). \tag{20}$$

System (15) then becomes:

$$\begin{cases} x'' + (1+y)x + \sqrt{\varepsilon}\left[(1-\sqrt{\varepsilon}\eta)^{1/2}\delta x^2 x' + \gamma(1-\sqrt{\varepsilon}\eta)x^3 - \eta(1+y)x\right] = 0, \\ y'' + 4y + \sqrt{\varepsilon}\left[b(1-\sqrt{\varepsilon}\eta)x^2 - 4\eta y + \sqrt{\varepsilon}\kappa(1-\sqrt{\varepsilon}\eta)^{1/2}y'\right] = 0, \end{cases} \tag{21}$$

where the accent denotes differentiation with respect the variable θ. Evidently, we have

$$\begin{cases} x_0(\theta) = x_{00}\text{MathieuS}(1, -c/2, \theta), \\ y_0(\theta) = c\cos 2\theta. \end{cases} \tag{22}$$

Note that the zero order solution is $\pi-$periodic in the variable θ. Solving the differential equation for $y_1(\theta)$ yields:

$$\begin{aligned} y_1(\theta) = & y_{10}\cos 2\theta + \frac{1}{2}\cos 2\theta \int_0^\theta \sin 2\tau \left[b x_0(\tau)^2 - 4\eta_0 y_0(\tau)\right] d\tau - \\ & \frac{1}{2}\sin 2\theta \int_0^\theta \cos 2\tau \left[b x_0(\tau)^2 - 4\eta_0 y_0(\tau)\right] d\tau. \end{aligned} \tag{23}$$

Requiring $y_1(\theta)$ to be $\pi-$periodic yields the following equations:

$$\begin{cases} \int_{-\frac{\pi}{2}}^{\frac{\pi}{2}} \sin 2\tau \left[bx_0(\tau)^2 - 4\eta_0 y_0(\tau) \right] d\tau = 0 \\ \int_{-\frac{\pi}{2}}^{\frac{\pi}{2}} \cos 2\tau \left[bx_0(\tau)^2 - 4\eta_0 y_0(\tau) \right] d\tau = 0 \end{cases} \tag{24}$$

The first periodicity condition is automatically satisfied because $x_0(t)$ is odd and $y_0(t)$ is even. Using the software package Maple, we find that the second periodicity condition becomes:

$$0.0400bx_{00}^2 - 80.8404\eta_0 = 0. \tag{25}$$

Collecting $O(\sqrt{\varepsilon})$ terms from the first equation of system (21) yields the following differential equation for $x_1(\theta)$.

$$\begin{cases} x_1'' + (1+y_0)x_1 + \left[x_0 y_1 + \delta x_0^2 x_0' + \gamma x_0^3 - \eta_0(1+y_0)x_0 \right] = 0, \\ x_1(0) = xx_{10}, \quad x_1'(0) = x_{10}. \end{cases} \tag{26}$$

This initial value problem has the following solution

$$\begin{aligned} x_1(\theta) =& xx_{10}\text{MathieuC}(1,-c/2,\theta) + x_{10}\text{MathieuS}(1,-c/2,\theta) - \\ & \text{MathieuS}(1,-c/2,\theta)\int_0^\theta \text{MathieuC}(1,-c/2,\tau)g(\tau)d\tau + \\ & \text{MathieuC}(1,-c/2,\theta)\int_0^\theta \text{MathieuS}(1,-c/2,\tau)g(\tau)d\tau, \end{aligned} \tag{27}$$

where

$$g(t) := \left[x_0(t)y_1(t) + \delta x_0^2(t)x_0'(t) + \gamma x_0^3(t) - \eta_0(1+y_0(t))x_0(t) \right],$$

and $\text{MathieuC}(1,-c/2,t)$ is defined as the solution of the following initial value problem:

$$\begin{cases} \ddot{x} + (1 + c\cos 2t)x = 0, \\ x(0) = 1, \quad \dot{x}(0) = 0. \end{cases} \tag{28}$$

Note that $\text{MathieuC}(1,-c/2,t)$ is even and not periodic.
Imposing the periodicity condition on x_1 yields, after some simplifications:

$$\begin{cases} x_{00}\left[0.0400y_{10} + 0.0056\gamma x_{00}^2 - 0.0005bx_{00}^2 \right] = 0, \\ x_{00}\left[0.02411\delta x_{00}^2 - 1.0403\gamma x_{00}^2 + 0.1014bx_{00}^2 - 7.4005y_{10} \right] = \\ xx_{10}\text{MathieuC}'(1,-c/2,\pi). \end{cases} \tag{29}$$

Combining equations (25) and (29), we can express all the unknowns in terms of x_{00}. We find:

$$\begin{cases} \eta_0 = 4.9444 \times 10^{-3} bx_{00}^2, \\ y_{10} = (0.0137b - 0.1406\gamma)x_{00}^2, \\ xx_{10} = (6.5096 \times 10^{-5}\delta - 7.7861 \times 10^{-6}\gamma)x_{00}^3, \end{cases} \tag{30}$$

with x_{00} still free to choose. One must go one order higher to determine x_{00}. Repeating the same procedure by collecting $O(\varepsilon)$ terms, solving the differential equations and imposing the periodicity condition yields four algebraic equations. One of them involves x_{00} only. We find

$$x_{00} = \sqrt[4]{\frac{\kappa\pi c}{2b\left[-5.3712\times10^{-4}\delta + 1.9710\times10^{-6}\gamma\right]}}. \tag{31}$$

Substituting the parameter values used in the numerical continuation, we find:

$$x_{00} = 24.7813, \quad \eta_0 = -0.076, \quad y_{10} = -23.6849, \quad \text{and} \quad xx_{10} = 0.3666. \tag{32}$$

This yields the following approximation of the $\pi-$periodic solutions:

$$x(\theta) = 24.7813\text{MathieuS}(1, -c/2, \theta) + O(\sqrt{\varepsilon}), \tag{33}$$

$$\begin{aligned} y(\theta) =& c\cos 2\theta - 23.6849\sqrt{\varepsilon}\Bigg[\cos 2\theta + \\ & \frac{1}{2}\cos 2\theta \int_0^\theta \sin 2\tau \left[bx_0(\tau)^2 - 4\eta_0 y_0(\tau)\right] d\tau - \\ & \frac{1}{2}\sin 2\theta \int_0^\theta \cos 2\tau \left[bx_0(\tau)^2 - 4\eta_0 y_0(\tau)\right] d\tau\Bigg] + O(\varepsilon) \end{aligned} \tag{34}$$

From equation (33), one easily computes the amplitude of the $x-$oscillator numerically. We find $[x] = 7.065$. This is in complete agreement with Fig. 13. To get the asymptotic expansion for the original system (1), one should multiply equation (33) by $\varepsilon^{1/4}$ to obtain

$$x(\theta) = 24.7813\text{MathieuS}(1, -c/2, \theta)\varepsilon^{1/4} + O(\varepsilon^{3/4}), \tag{35}$$

$$\begin{aligned} y(\theta) =& c\cos 2\theta - 23.6849\sqrt{\varepsilon}\Bigg[\cos 2\theta + \\ & \frac{1}{2}\cos 2\theta \int_0^\theta \sin 2\tau \left[bx_0(\tau)^2 - 4\eta_0 y_0(\tau)\right] d\tau - \\ & \frac{1}{2}\sin 2\theta \int_0^\theta \cos 2\tau \left[bx_0(\tau)^2 - 4\eta_0 y_0(\tau)\right] d\tau\Bigg] + O(\varepsilon) \end{aligned} \tag{36}$$

$$T = \pi\left(1 + 0.038\sqrt{\varepsilon} + O(\varepsilon)\right), \tag{37}$$

where T denotes the period of the solution of the original system (1).

Conclusion

Using a combination of numerical and analytical continuation, we were able to understand the origin and nature of the $\pi-$periodic solutions found

numerically, see Fig. 12. The scaling used to pinpoint the periodic solutions is in this case not trivial. It turns out the amplitude of the $x-$oscillator is $O(\varepsilon^{-1/4})$.

5.3 Bifurcation analysis of the π-cycle

A backward continuation of the π-cycle yields a fold bifurcation at $\gamma = 0.23935$ and at $\gamma = 0.25518$, as we hit the left and the right side of the fold curve (**Fold2**) respectively. The stable cycle emerging after the second hit undergoes a Neimark-Sacker bifurcation at $\gamma = 0.23189$ yielding a torus. When we perform a forward continuation of the π-periodic solution with respect to the parameter γ, the cycle undergoes a fold bifurcation at $\gamma = 0.29282$. Here, we hit the curve (**Fold1**). The unstable cycle emerging after this fold bifurcation undergoes a period-doubling bifurcation at $\gamma = 0.11946$. As before, we use the parameter b as a second control parameter to generate the full bifurcation diagram. See Fig. 14 below.

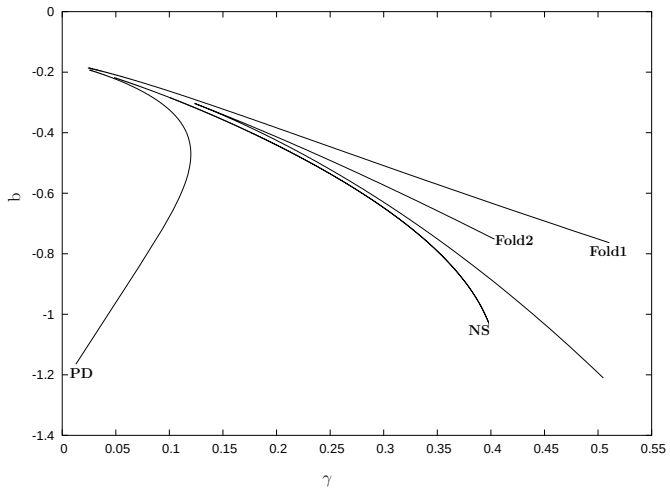

Figure 14: Bifurcation diagram of the π-periodic cycle.

A frequence sweep, keeping $b = -0.5$ and varying the parameter γ yields many phase-lockings while crossing a number of Arnold tongues. Consider for example a period 10 solution and a period 32 solution in Fig. 15.

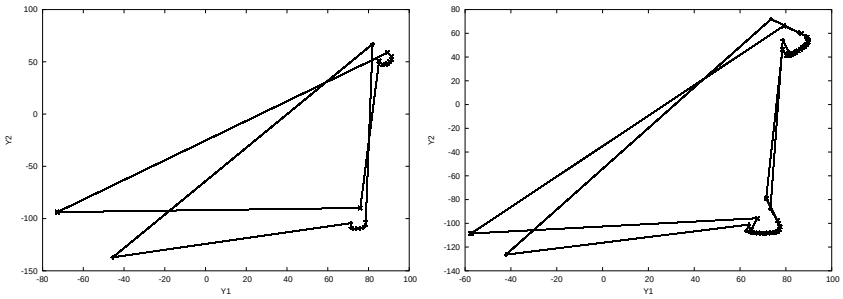

Figure 15: Projection of Poincaré map on the y_1y_2 plane of period 10 and a period 32 solutions at respectively $\gamma = 0.2239$ and $\gamma = 0.2272$. To indicate the dynamics, the transition points of the maps have been connected by straight lines.

The torus emerging after the Neimark-Sacker bifurcation also becomes resonant and gets destroyed according to a scenario similar to the one described in the preceding section. Two symmetrically coupled strange attractors are born. If we continue decreasing the parameter γ, the two attractors begin to interact yielding the strange attractor shown in Fig. 16 below. One identifies the remains of the two symmetrical tori. The orbits in the strange attractor oscillate randomly between these two objects. This is geometrically reminiscent of the Lorenz attractor.
The 2π unstable cycle emerging from the period doubling bifurcation becomes a neutral saddle at $\gamma = 0.08679$. It is suggested by a number of numerical integrations, that this 2π-cycle interacts somehow with the strange attractor in Fig. 3 yielding a large strange attractor, see Fig. 17. But, further study is clearly necessary to better understand how the strange attractor evolves and what kind of interactions are involved in this evolution.

6 Discussion and conclusions

1. The phenomena, described here for dynamical system (1), are within reach of the various analytic and numerical techniques used in this paper. Averaging-normalisation helps as it produces relative equilibria corresponding with periodic solutions. Equilibria and their bifurcations to periodic solutions which should be called 'relative periodic solutions' as they correspond with tori, are easier to analyse by numerical bifurcation techniques than the tori of the original system.

2. We can not expect to have a *complete* description of all qualitatively different phenomena of system (1). We have described a prominent one, the $1:6$ resonance tongue and its associated scenarios, but other phenomena can be found, for instance at a larger distance from the

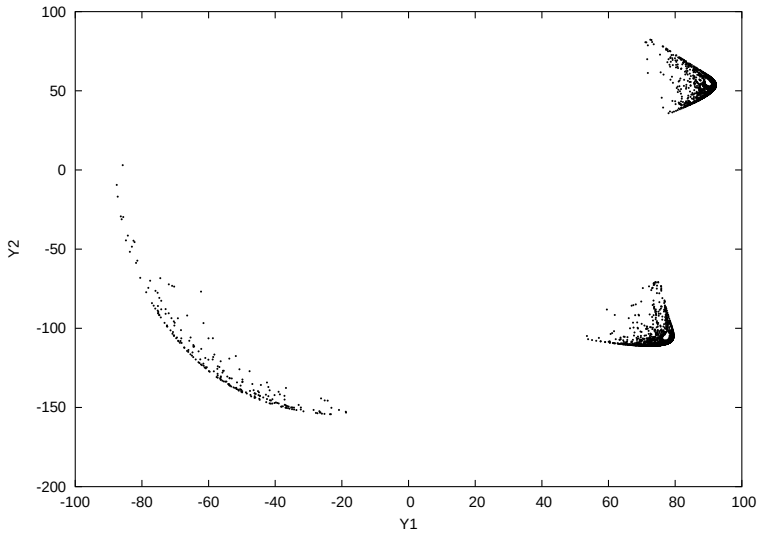

Figure 16: Projection of Poincaré section, using $\Sigma = \{(0, x_2, y_1, y_2)^T, x_2, y_1, y_2 \in \mathbb{R}\}$ as cross section, projected onto the y_1y_2 plane with $\gamma = 0.22$. The closed curve no longer exists. A strange attractor emerges instead. Kaplan-Yorke dimension $d_{KY} \approx 2.90$.

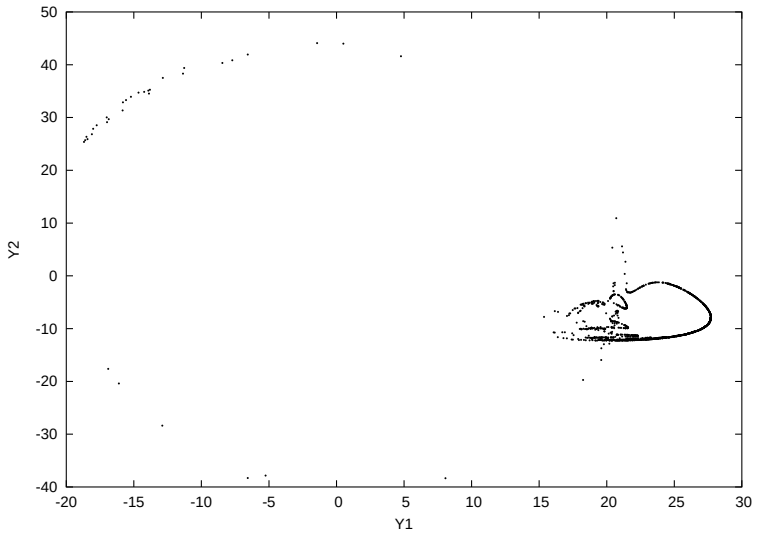

Figure 17: Poincaré section, using $\Sigma = \{(0, x_2, y_1, y_2)^T, x_2, y_1, y_2 \in \mathbb{R}\}$ as cross section, projected onto the y_1y_2 plane with $\gamma = 0.089$. The strange attractor in Fig. 3 interacts with other regimes. Kaplan-Yorke dimension $d_{KY} \approx 2.37$.

origin. In particular the problem of possible interaction of attractors as shown in Fig. 17 poses an interesting open problem.

3. The genericity of the phenomena discussed here, should be more explored. In any case, putting the damping coefficients δ, κ zero, will produce non-generic phenomena.

4. This paper can be seen as an illustration of the Ruelle-Takens scenario [22], [23], where it is argued that an equilibrium can produce a periodic solution by Hopf bifurcation, followed in subsequent bifurcation by a torus. As stated in [22] (section 9): "a quasi-periodic flow on a torus gives flows with strange attractors and more generally, flows which are not Morse-Smale."

5. At the end of appendix 2, we conjecture that countably many $l\pi$-periodic solutions exist. The analytic and numerical evidence for this is strongly suggestive but not conclusive.

7 Acknowledgments

The mechanics model studied in this paper was designed by A. Tondl (Prague, Czech Republic). Discussions with Yu.A. Kuznetsov and J.J. Duistermaat are gratefully acknowledged. H.W. Broer supplied us with valuable comments on an earlier version of the paper.

Appendix 1 on the stability of the periodic solution

Proposition 4 *The nontrivial critical point of system (11) is asymptotically stable in parameter space* $\kappa,\ \delta > 0,\ b < -2\delta\kappa$.

Proof. We use the Routh-Hurwitz criterion, see [14], to establish the parameter range within which asymptotic stability holds. A necessary and sufficient condition for asymptotic stability reduces in our case to the following:

$$\begin{cases} \Delta_1 & = \kappa + \dfrac{\delta R_{1a}^2}{2} > 0; \\ \Delta_2 & = -\dfrac{b}{4\kappa} + \dfrac{\kappa}{16}(b + 8\delta\kappa)R_{1a}^2 + \dfrac{\delta^2\kappa}{16}R_{1a}^4 - \dfrac{b\delta^2}{64\kappa}R_{1a}^6 > 0; \\ \Delta_3 & = b_3\Delta_2 > 0. \end{cases} \tag{38}$$

Where,

$$b_3 = \frac{b\sin 2\theta R_{1a}^4}{256\kappa}(12\kappa\gamma - b\sin 2\theta).$$

One can easily establish that $b_3 > 0$. This follows from system (12) and the fact that $\theta \in (\pi/2, \pi)$. The first equation is, in our case, automatically satisfied. This way the stability condition reduces to $\Delta_2 > 0$. We will in our proof distinguish between two complementary cases.

The case $b + 8\delta\kappa \geq 0$

From (38) we have that the second equation is satisfied as all the coefficients of R_{1a}^{2i}, $i = 0, \cdots, 3$ are positive.

The case $b + 8\delta\kappa < 0$

We consider here Δ_2 as a function of the parameter γ which is hidden in R_{1a} only and estimate its minimum value with respect to the parameter γ. First we write Δ_2 as follows:

$$\Delta_2 = A - BR_1(\gamma)^2 + CR_1(\gamma)^4 + DR_1(\gamma)^6.$$

Where A, B, C, and $D > 0$ and independent of γ. Taking the derivative with respect to the parameter γ gives:

$$\dot{\Delta}_2 = 2R_1\dot{R}_1(-B + 2CR_1^2 + 3DR_1^4).$$

From equation (12) we see that $\dot{R}_1 < 0$. As $\dot{R}_1 < 0$ and $R_1 > 0$ for all values of γ, we can easily show by analysing the sign of $\dot{\Delta}_2$ that Δ_2, as a function of γ, has one extremum which is a global minimum. We find, after some simplifications, the following expression for the minimum:

$$\Delta_{min} = \frac{-\kappa^2(b + 2\delta\kappa)}{72b^2\delta}\left(9b^2 + 2b(Q - 18\delta\kappa) + 12\delta\kappa(Q - 6\delta\kappa)\right),$$

where

$$Q = \sqrt{3(b + 4\delta\kappa)^2 - 12\delta^2\kappa^2}.$$

Notice that the quantity $-\kappa^2(b + 2\delta\kappa)/(72b^2\delta)$ is positive in the case $b + 8\delta\kappa < 0$. It is also easy to show that

$$6\delta\kappa < Q < -\sqrt{3}(b + 4\delta\kappa)$$

This follows essentially from the fact that $b + 8\delta\kappa < 0$. With these estimates we can give a lower bound for Δ_{min}. We find

$$\Delta_{min} > \frac{-\kappa^2(b + 2\delta\kappa)}{72b^2\delta}\left((9 - 2\sqrt{3})b^2 - 2(18 + 4\sqrt{3})\kappa\delta b\right) > 0$$

This concludes the proof.

Appendix 2 on Mathieu-functions and the PL-method

To obtain the equations of the PL-method in section 5.2, we used some results regarding Mathieu functions; we mention briefly:

Proposition 5 *Suppose that for some value of the parameter c the function MathieuS$(1, c, t)$ is $\pi-$periodic. Then the following holds*

1. *MathieuC$(1, c, t)$ is not periodic.*
2. *MathieuC$(1, c, k\pi) = 1$, for all $k \in \mathbb{Z}$.*
3. *MathieuC$(1, c, t + k\pi) =$ MathieuC$(1, c, t) +$ kMathieuC$'(1, c, \pi)$ MathieuS$(1, c, t)$, for all $k \in \mathbb{Z}$.*
4. *MathieuC$'(1, c, \pi) \neq 0$.*

The second item is a direct consequence of the Wronski-determinant of the Mathieu equation being time-independent. The third item is a consequence of the second item and the fact that MathieuC$(1, c, t + k\pi)$ is a solution of the Mathieu equation as well. The fourth item is a direct consequence of the first and third item. The first item is a consequence of Floquet's theorem. When applied to the Mathieu equation, we have the usual Floquet decomposition $\phi(t) = P(t)exp.(tB)$, *characteristic multipliers* and *characteristic exponents* (eigenvalues of B). When the characteristic exponents are an integer multiple of i, one can show that the matrix B is not diagonalisable leading to one periodic solution and the other being a polynomial times a periodic solution. In the case studied with the PL-method, we have that a characteristic exponent equals $2i$. This explains why the MathieuC$(1, c, t)$ cannot be periodic when MathieuS$(1, c, t)$ is $\pi-$periodic. According to Floquet theory, the unperturbed system (15) with $\varepsilon = 0$ does have, for each integer k, countably many periodic solutions with period equal to $k\pi$. One can try to continue each of those periodic solutions using the PL-method. If the algebraic system obtained by this method is non-trivially solvable, then the periodic solution can be continued with respect to the parameter ε and consequently the original system (1) with $a = 1$ will have a periodic solution as well.

We find that the numerical bifurcation analysis and the PL-continuation method are in agreement. We formulate a conjecture as follows:

Conjecture 1 *For any integer l, system (1) with $a = 1$, $b < -2\kappa\delta < 0$ has countably many $l\pi-$periodic solutions with $x(t) = O(\kappa^{1/4})$ and $y(t) = O(1)$ when κ tends to zero.*

References

[1] V.S. Afraimovich, L.P. Shil'nikov, *Invariant Two-Dimensional Tori, Their Breakdown and Stochasticity*, Amer. Math. Soc. Trans. (2) Vol. 149, 1991.

[2] V.I. Arnol'd, *Dynamical Systems V*, Springer, Berlin, 1994.

[3] D.G. Aronson, M.A. Chory, G.R. Hall, R.P. McGehee, *Bifurcations from an Invariant Circle for Two-Parameter Families of Maps of the Plane: A computer-assisted study*, Commun. Math. Phys. 83 (1982), 303–354.

[4] C. Baesens, J Guckenheimer, S. Kim and R.S. Mackay, *Three coupled oscillators: mode-locking, global bifurcations and toroidal chaos*, Physica D 49, 387-475 (1991).

[5] T. Bakri, R. Nabergoj, A. Tondl, F. Verhulst, *Parametric Excitation in Non-linear Dynamics*, International Journal of Non-Linear Mechanics 39 (2004) 311–329.

[6] H. Broer, C. Simó, J.C. Tatjer, *Towards global models near homoclinic tangencies of dissipative diffeomorphisms*, Nonlinearity 11 (1998) 667–770.

[7] H. Broer, M.B. Sevryuk, *KAM Theory: quasi-periodicity in dynamical systems*, in Handbook of Dynamical Systems 3 (H.W. Broer, B. Hasselblatt, F. Takens, eds.) (2010) 249–344.

[8] H.W. Broer, *Resonance and fractal geometry*, Acta Applicandae Mathematicae (2012), http://dx.doi.org/10.1007/s10440-012-9670-x.

[9] F. Della Rossa, V. De Witte, W. Govaerts and Yu.A. Kuznetsov, *Numerical periodic normalization for codim 2 bifurcations of limit cycles*, 90p. Preprint arXive http://arxiv.org/pdf/1111.4445v1.pdf (2011).

[10] A. Dhooge, W. Govaerts and Yu.A. Kuznetsov, MATCONT*: A MATLAB package for numerical bifurcation analysis of ODEs*, ACM Trans. Math. Software 29, pp. 141 - 164 (2003).

[11] A. Dhooge, W. Govaerts, Yu.A. Kuznetsov, H.G.E. Meijer and B. Sautois, *New features of the software* MATCONT *for bifurcation analysis of dynamical systems*, Mathematical and Computer Modelling of Dynamical Systems 14, pp. 145-175 (2008).

[12] E.J. Doedel, R.C. Paffenroth, A.R. Champneys, T.F. Fairgrieve, Y.A. Kuznetsov, B. Sandstede, X. Wang, *Auto 2000: Continuation and Bifurcation Software for Ordinary Differential Equations*. `http://sourceforge.net/projects/auto2000`.

[13] O.G. Galkin, *Resonance regions for Mathieu type dynamical systems on a torus*, Physica D, (1989) 287–298.

[14] F.R. Gantmacher (1959), *Applications of the theory of matrices*, Interscience, Dover reprint, New York.

[15] J.K. Hale (1969), *Ordinary Differential Equations*, John Wiley.

[16] B. Krauskopf, H. Osinga, *Growing 1D and Quasi-2D Unstable Manifolds of Maps*, Journal of Computational Physics 146, (1998) 404–419.

[17] Yu.A. Kuznetsov, *Elements of Applied Bifurcation Theory*, 2nd rev. ed., Springer, New York, 1995.

[18] Yu.A. Kuznetsov, V.V. Levitin, 1997. CONTENT: A multiplatform environment for analysing dynamical systems. Dynamical Systems Laboratory, Centrum voor Wiskunde en Informatica, Amsterdam, `http://www.math.uu.nl/people/kuznet/CONTENT/`.

[19] R. Lin, C.W.S. To, K.L. Huang, Q.S. Lu, *Secondary Bifurcations of Two Non-Linearly Coupled Oscillators*, Journal of Sound and Vibrations (1993) 165(2), 225–250.

[20] The program MATCONT is freely available for download from: `http://allserv.rug.ac.be/~ajdhooge`

[21] J. Palis and F. Takens, *Hyperbolicity and sensitive chaotic dynamics at homoclinic bifurcations*, Cambridge University Press (1993).

[22] D. Ruelle and F. Takens, *On the nature of turbulence*, Comm. Math. Physics 20, 167-192 (1971) and 23, 241-248 (1971).

[23] D. Ruelle , *Differentiable dynamical systems and the problem of turbulence*, Bull. AMS 5, pp. 29-42 (1981).

[24] J.A. Sanders, F. Verhulst and J. Murdock, *Averaging Methods in Nonlinear Dynamical Systems*, 2d rev. ed., Applied mathematical Sciences 59, Springer, New York (2007).

[25] F. Schilder, H.M. Osinga and W. Vogt, *Continuation of quasi-periodic invariant tori*, SIAM J. Appl. Dyn. Syst., 4(3), pp. 459488 (2005).

[26] F. Schilder, W. Vogt, S. Schreiber and H.M. Osinga, *Fourier methods for quasi-periodic oscillations*, J. Numer. Meth. Engng 67, 629-671 (2006).

[27] F. Schilder and B.B. Peckham, *Computing Arnold tongue scenarios*, J. Computational Physics 220, 932-951 (2007).

[28] A. Shilnikov, L.P. Shilnikov, D. Turaev, *On some mathematical topics in classical synchronisation. A tutorial*, International Journal of Bifurcation and Chaos, Vol. 14,(7) (2004) 2143–2160.

[29] L. van Veen, *Time scale interaction in low-order climate models*, Ph.D. thesis, Mathematics Institute, Utrecht University, the Netherlands, 2002.

[30] F. Verhulst, *Nonlinear Differential Equations and Dynamical Systems*, Springer, Berlin, Heidelberg, 1996.

[31] R. Vitolo, *Bifurcations of attractors in 3D diffeomorphisms*, Ph.D. thesis, University of Groningen, the Netherlands, 2003.

[32] R. Vitolo, H.W. Broer and C. Simó *Quasi-periodic bifurcations of invariant circles in low-dimensional dissipative dynamical systems*, Regular and Chaotic Dynamics 16 (2011), 154-184.